# Drift-Free Current Sensorless MPPT Algorithm in Photovoltaic Systems

Xingshuo Li, Huiqing Wen, Lin Jiang, Yihua Hu

**Abstract**

High system cost and reduced output power due to the changing weather conditions such as the irradiance or temperature are two major concerns for a practical photovoltaic (PV) system design. This paper presents a current sensorless (CS) maximum power point tracking (MPPT) algorithm that uses only one single-input-voltage sensor (SIVS) and totally eliminates the expensive current sensors, which can significantly reduce the system cost and retain the advantages of the widely used MPPT algorithms such as incremental conductance (INC). To further eliminate the drift effect, which is a severe phenomenon due to the incorrect decision in duty cycle for fast irradiation change, drift-free technique is adopted in the presented algorithm by incorporating the information of change in duty cycle ($\Delta$D) and change in input voltage ($\Delta$V). A mathematical expression is given to define the drift-free criterion and the threshold is determined by the Lambert W function with respect to the dynamic EN50530 test standard. Experimental results under different scenarios are presented to validate the advantages of the presented method in terms of the tracking efficiency and drift-free characteristic.

**Index Terms**

Maximum power point tracking (MPPT), photovoltaic (PV) system, current sensorless, drift phenomena.

## I. Introduction

High system cost is one of major obstacles for the large-scale application of photovoltaic (PV) energy. Although the price of PV modules has experienced a substantial decrease during the past 20 years, the grid parity of PV power has not been fulfilled in most countries [10]. Furthermore, since the actual power yield of PV systems is highly dependent on the environmental conditions such as solar irradiance and temperature, the maximum power under any environmental condition is difficult to achieve for a practical photovoltaic (PV) system without the maximum power point tracking (MPPT) techniques. So far, many MPPT techniques have been discussed by [6, 13, 23], such as perturb and observe (P&O)

[1, 8, 9], incremental conductance (INC) [28, 30], fuzzy-logic controller (FLC) method [17, 22], MPP-Locus method [31, 33] and beta method [18, 19]. However, in order to implement these MPPT techniques, both current and voltage sensors are normally required, which increase the system cost. Thus, in order to address the concerns of a practical PV system design such as high system cost and reduced actual power yield, it is meaningful to find new MPPT techniques with good tracking performance and low number of sensors .

Recently many sensorless MPPT techniques have been discussed. According to the sensors eliminated, basically the sensorless MPPT techniques can be categorized into two groups: one is the current sensorless (CS) MPPT methods [5, 7, 11, 14, 15, 20, 21, 26, 34], which reduce the current sensors; and the other is the voltage-sensorless (VS) MPPT methods [12, 24, 25, 29], which reduce the voltage sensors. For the MPPT application, the current sensors can be a Hall-effect structure or a shunt resistor with differential amplifier configuration, which are usually expensive, complex, limited bandwidth, and possible noise-sensitive, while the voltage sensors are much cheaper and simpler compared with current sensors since they only require a voltage divider circuit [15]. Therefore, compared to the VS MPPT methods, the CS MPPT methods are preferable due to lower cost and higher efficiency.

According to the number and position of the voltage sensor, the current sensorless MPPT methods can be further divided into two sub-groups: one is the single-input-voltage-sensor (SIVS) MPPT methods [5, 7, 11, 15, 21, 34], and the other is the input and output voltage sensor (IOVS) MPPT methods [14, 20, 26]. For the IOVS methods, the input voltage, output voltage and the duty cycle of the dc-dc converter are used to estimate the input current. Then, the estimated input current and measured input voltage can be used to track the maximum power point (MPP) by implementing the conventional MPPT methods, such as P&O method and INC method. However, since the IOVS methods require two voltage sensors, their cost is still high. Compared to the IOVS methods, the SIVS methods only require one voltage sensor. Furthermore, unlike the IOVS methods, the SIVS methods can directly track the MPP by using the relationship between the duty cycle of the dc-dc converter and input voltage [21, 34]. Besides, a variable step size can be integrated into the SIVS methods [7, 11, 15] to obtain a fast tracking speed and reduced steady-state oscillations.

Another problem for the widely-used classical MPPT methods such as the P&O method and the INC method is the drift phenomenon, which is frequently occurred due to the misjudgment of MPPT algorithms under the condition of a rapid change in irradiation. As a consequence, the system operating point will be drifted away from the true MPP when the misjudgement of MPPT methods happen. Although some modified MPPT methods have been discussed to address this problem [16, 27, 32], the current sensors are necessary. For the SIVS current sensorless MPPT algorithm, the drift problem may also happen, and

the solutions adopted by conventional MPPT methods in [16, 27, 32] are unable to solve this issue due to the elimination of current sensors. Although one of the SIVS method claims that this method is free from drift for both of increase and decrease in solar irradiance [15], the criteria for the drift avoidance have not been given. Furthermore, due to the lack of consideration in the changes of duty cycle, this method is actually unable to completely avoid the drift phenomena. As a matter of fact, as shown in this paper, the drift phenomenon by using the SIVS method in [15] may also happen under the analyzed scenarios and the probability is close to 50% for both the increase and decrease in solar irradiance.

In this paper, the drift phenomenon for the SIVS current sensorless MPPT algorithms is studied, and a novel drift-free current sensorless MPPT algorithm is presented to reduce the system cost and solve the drift problem. The drift-free criterion is given with the mathematical expression. Furthermore, the threshold is determined by the Lambert W function with respect to the dynamic EN50530 test standard. The presented MPPT algorithm will result in reduced costs and circuit complexity. Besides, it has operation characteristics similar to those of the INC algorithm in terms of the tracking time and MPPT efficiencies. In order to validate the advantages of the presented method, experimental results under various of cases are illustrated.

## II. Review of the Conventional SIVS Current Sensorless Method

The principle of the SIVS method is to obtain the relationship between the duty cycle of the dc-dc converter and input voltage based on the dc-dc converter topology [34]. Taking a boost converter as an example, the relationship between the input voltage $V_{pv}$ and output voltage $V_o$ is given by

$$V_o = \frac{V_{pv}}{1-D} \tag{1}$$

where $D$ refers to the duty cycle of the boost converter.

According to the previous research, there are two ways to obtain this relationship. In [34], the determination of this relationship is based on the output power of the boost converter $P_o$, which is given as

$$P_o = \frac{V_o^2}{R_L} \tag{2}$$

where $R_L$ refers to the load resistance. At the MPP, the derivative of $P_o$ versus time should be equal to zero, thus:

$$\frac{\mathrm{d}P_o}{\mathrm{d}t} = \frac{\mathrm{d}V_o}{\mathrm{d}t} = 0 \tag{3}$$

Substituting (1) into (3), it is given as

$$\frac{\mathrm{d}V_o}{\mathrm{d}t} = \frac{\mathrm{d}(V_{pv}/(1-D))}{\mathrm{d}t} \tag{4}$$

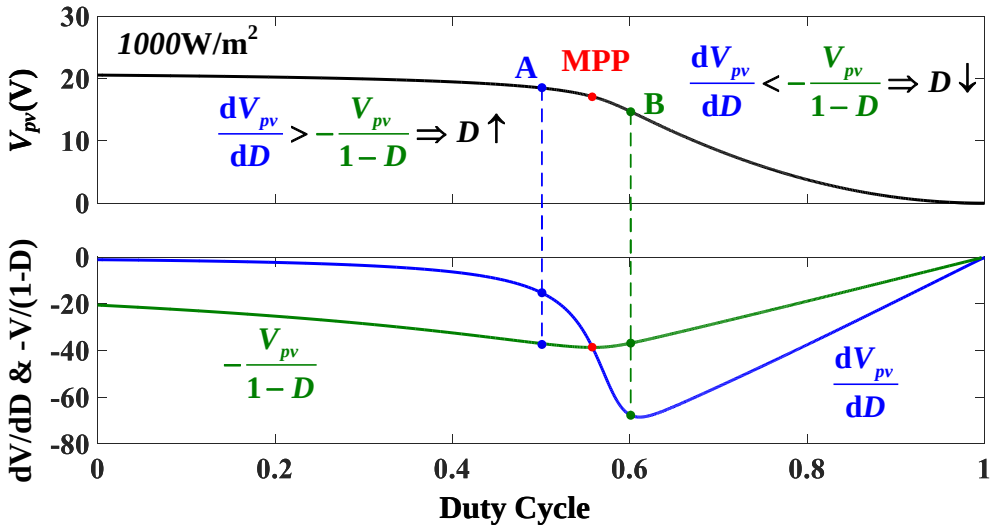


Fig. 1. The characteristics of voltage and duty cycle for the boost converter.

Then, simplifying (4), we have

$$\frac{\mathrm{d}V_{pv}}{\mathrm{d}D} = -\frac{V_{pv}}{1-D} \tag{5}$$

From Fig. 1, it can be seen that the term $\mathrm{d}V_{pv}/\mathrm{d}D$ equals to the term $-V_{pv}/(1-D)$ at the MPP. When the term $\mathrm{d}V_{pv}/\mathrm{d}D$ is larger than the term $-V_{pv}/(1-D)$, $D$ should be increased towards the MPP. By contrast, when the term $\mathrm{d}V_{pv}/\mathrm{d}D$ is smaller than the term $-V_{pv}/(1-D)$, $D$ should be decreased. Therefore, this relationship can be summarized as below:

$$\begin{cases} \dfrac{\mathrm{d}V_{pv}}{\mathrm{d}D} > -\dfrac{V_{pv}}{1-D}, & D\uparrow \quad (6a) \\ \dfrac{\mathrm{d}V_{pv}}{\mathrm{d}D} = -\dfrac{V_{pv}}{1-D}, & \text{At MPP} \quad (6b) \\ \dfrac{\mathrm{d}V_{pv}}{\mathrm{d}D} < -\dfrac{V_{pv}}{1-D}, & D\downarrow \quad (6c) \end{cases}$$

In [15], another way to obtain the relationship is given, which is based on the input power $P_{pv}$ as shown below:

$$P_{pv} = \frac{V_{pv}^2}{R_{pv}} \tag{7}$$

where $R_{pv}$ is the equivalent input resistance.

Then, assuming $\eta$ is the efficiency of the boost converter, which can be expressed as:

$$\eta = \frac{P_o}{P_{pv}} = \frac{V_o^2/R_L}{V_{pv}^2/R_{pv}} = \left(\frac{V_o}{V_{pv}}\right)^2 \frac{R_{pv}}{R_L} \tag{8}$$

Substituting (1) into (8), the expression can be obtained as:

$$R_{pv} = \eta \left(\frac{1}{1-D}\right)^2 R_L \tag{9}$$

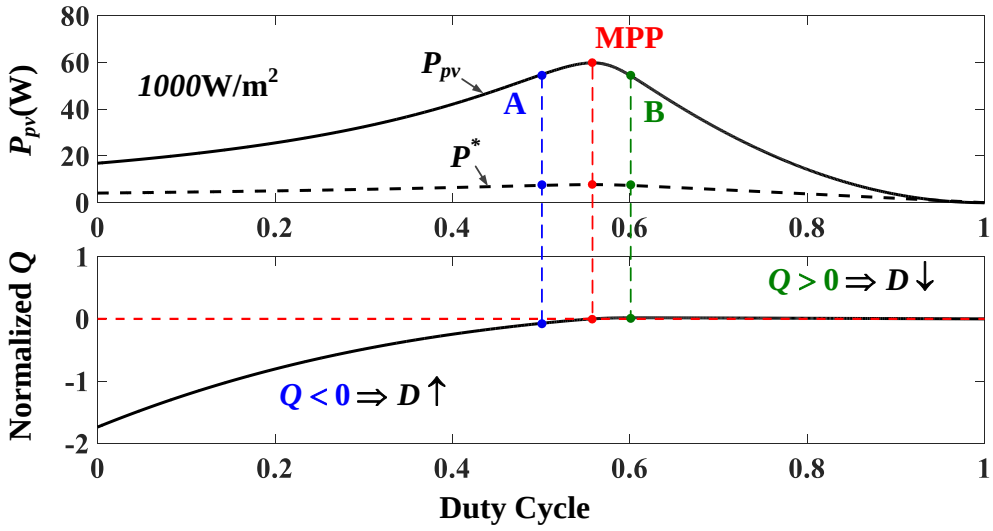


Fig. 2. $P$-$D$ and $P^*$-$D$ characteristics, and the normalized $Q$ versus $D$ for the boost converter.

Then, substituting (9) into (7), the following expression can be obtained as:

$$P_{pv} = \frac{V_{pv}^2}{\eta R_L}\left(\frac{1}{1-D}\right)^2 \tag{10}$$

Extracting a square root of (10), it is given as

$$P^* = \sqrt{P_{pv}} = \frac{V_{pv}}{\sqrt{\eta R_L}}\left(\frac{1}{1-D}\right) \tag{11}$$

Fig. 2 shows the $P$-$D$ and $P^*$-$D$ characteristics of the boost converter. As shown in Fig. 2, the slopes of the $P$-$D$ curve and $P^*$-$D$ curve should be equal to zero. Hence, the derivative of $P^*$ versus $D$ equals zero:

$$\begin{aligned}\frac{\mathrm{d}P^*}{\mathrm{d}D} &= \left(V_{pv}\frac{1}{(1-D)^2} + \frac{1}{1-D}\frac{\mathrm{d}V_{pv}}{\mathrm{d}D}\right)\frac{1}{\sqrt{\eta R_L}} \\ &= \left(\frac{V_{pv}\mathrm{d}D + (1-D)\mathrm{d}V_{pv}}{(1-D)^2\mathrm{d}D}\right)\frac{1}{\sqrt{\eta R_L}} = 0\end{aligned} \tag{12}$$

Finally, an objective function Q can be obtained as follow:

$$Q = (1-D)\mathrm{d}V_{pv} + V_{pv}\mathrm{d}D \begin{cases} < 0, \ D\uparrow & \text{(13a)} \\ = 0, \ \text{At MPP} & \text{(13b)} \\ > 0, \ D\downarrow & \text{(13c)} \end{cases}$$

From Fig. 2, it can be seen that $Q$ is equal to zero at the MPP. When $Q$ is positive, $D$ should be decreased, and vise versa.

TABLE I

SUMMARIZATION OF VOLTAGE CONVERSION RATIO, TERMS IN (6) AND $Q$ FOR DIFFERENT DC-DC CONVERTERS

| Converter | $M(d)$ | Terms in (6) | $Q$ |
|---|---|---|---|
| Buck | $d$ | $\frac{\mathrm{d}V_{pv}}{\mathrm{d}D} = -\frac{V_{pv}}{D}$ | $Q = D\mathrm{d}V_{pv} + V_{pv}\mathrm{d}D$ |
| Boost | $\frac{1}{1-d}$ | $\frac{\mathrm{d}V_{pv}}{\mathrm{d}D} = -\frac{V_{pv}}{1-D}$ | $Q = (1-D)\mathrm{d}V_{pv} + V_{pv}\mathrm{d}D$ |
| Buck-Boost | $-\frac{d}{1-d}$ | $\frac{\mathrm{d}V_{pv}}{\mathrm{d}D} = -\frac{V_{pv}}{D(1-D)}$ | $Q = D(1-D)\mathrm{d}V_{pv} + V_{pv}\mathrm{d}D$ |
| Cuk | $-\frac{d}{1-d}$ | $\frac{\mathrm{d}V_{pv}}{\mathrm{d}D} = -\frac{V_{pv}}{D(1-D)}$ | $Q = D(1-D)\mathrm{d}V_{pv} + V_{pv}\mathrm{d}D$ |
| SEPIC | $\frac{d}{1-d}$ | $\frac{\mathrm{d}V_{pv}}{\mathrm{d}D} = -\frac{V_{pv}}{D(1-D)}$ | $Q = D(1-D)\mathrm{d}V_{pv} + V_{pv}\mathrm{d}D$ |

From the aforementioned discussion, the SIVS method based on (6) has operation characteristics similar to the INC method, while the SIVS method based on (13) is similar to the P&O method. Furthermore, if the left-hand fraction in (6) cross-multiplies its right-hand one, thus:

$$(1-D)\mathrm{d}V_{pv} = -V_{pv}\mathrm{d}D \tag{14}$$

Then, move the right-hand term to the left-hand side, thus:

$$(1-D)\mathrm{d}V_{pv} + V_{pv}\mathrm{d}D = 0 \tag{15}$$

which is exactly same as (13b). In other words, the SIVS method based on (6) and (13) can be treated as the same method in different formats.

Furthermore, since the different dc-dc converters have different voltage conversion ratio $M(d)$, their corresponding terms in (6) and $Q$ are also different, which are summarized in TABLE I.

## III. DRIFT-FREE CURRENT SENSORLESS MPPT ALGORITHM

### *A. Drift Analysis with the conventional SIVS method*

In the previous research, the behaviors of the wrong step changes made by the P&O method and the INC method have been studied in [16, 27, 32], which refers to drift phenomenon. Generally, the drift for the P&O method and the INC method may happen when the solar irradiance suddenly increases. With the SIVS current sensorless MPPT, the drift phenomenon would also happen.

Fig. 3 shows the drift analysis for the SIVS method in [34], and Fig. 4 shows the simulation results for this method when the solar irradiance changes between $1000\mathrm{W/m}^2$ to $600\mathrm{W/m}^2$.

In Fig. 3 (a), initially, assuming that the operating point (OP) is located around the MPP. At time $t = 0.4s$, although the solar irradiance decreases from $1000\text{W/m}^2$ to $600\text{W/m}^2$, the duty cycle $D$ does not change at this time, as shown in Fig. 4 (a) and (b). Thus, the OP will directly move from the MPP to the point C. At the point C, $-V_{pv}/(1-D)$ is always negative, whose point is located on the dash green line and marked as orange color in Fig. 3 (a). However, the value of $\mathrm{d}V_{pv}/\mathrm{d}D$ depends on the changes of the duty cycle $D$ in the last perturbation. As shown in Fig. 4 (a) and (b), before the MPP moving to the point C, there are two possibilities for the changes of the duty cycle $D$: one is the last perturbation is from the point A to the MPP, while the other one is that from the point B to the MPP.

When the point A is perturbed to the MPP, the change of the duty cycle $D$ is positive. Since the change of $V_{pv}$ is always negative when the solar irradiance decreases, $\mathrm{d}V_{pv}/\mathrm{d}D$ will be negative. At this circumstance, (6c) is satisfied, so the duty cycle $D$ will be decreased. Then, the OP will move correctly to the point $\mathrm{C}_1$. By contrast, when the point B is perturbed to the MPP, both of the changes of the duty cycle $D$ and $V_{pv}$ is negative. As a consequence, $\mathrm{d}V_{pv}/\mathrm{d}D$ will be positive, marked as the point $\mathrm{C_B}$ with a green cross in Fig. 3 (a). At this time, (6a) is satisfied, so the duty cycle $D$ will be increased, and the OP will move to the point $\mathrm{C}_2$, which is drift away from the MPP.

When the solar irradiance increases from $600\text{W/m}^2$ to $1000\text{W/m}^2$, the OP will directly move from the MPP to the point C, as shown in Fig. 4 (c) and (d). Similar to the conditions that the solar irradiance decreases, $\mathrm{d}V_{pv}/\mathrm{d}D$ is always negative and there are also two possible values for $\mathrm{d}V_{pv}/\mathrm{d}D$. If the point A is perturbed to the MPP, (6c) is satisfied and the duty cycle $D$ will be increased. Hence, the OP will move correctly to the point $\mathrm{C}_1$. By contrast, when the point B is perturbed to the MPP, (6a) is satisfied and so the duty cycle $D$ will be decreased. Then, the OP will move to the point $\mathrm{C}_2$ and drift away from the MPP.

TABLE II summarizes the variation in $\mathrm{d}V$, $\mathrm{d}D$ and the duty cycle $D$ during the variation in solar irradiance for the SIVS method in [34]. Since the possibilities for the positive or negative $\mathrm{d}D$ are 50% during the system operation, the possibilities for the drift are also 50% during the variation in solar irradiance. As previously discussed in Section II, the SIVS method based on (6) and (13) can be treated as the same method. Therefore, $Q$ in (13) is also affected by the changes of the duty cycle $D$, its possibilities for the drift are also 50% for the variation in solar irradiance.

### *B. Novel MPPT Algorithm*

Fig. 5 shows the flowchart of the presented method. At the beginning, the presented method measures the present value of input voltage $V(\mathrm{k})$. Then, the present value of duty cycle $D(\mathrm{k})$, the previous values of the input voltage $V(\mathrm{k}-1)$ and duty cycle $D(\mathrm{k}-1)$ are read to calculate $\mathrm{d}V$ and $\mathrm{d}D$. (6) is used to

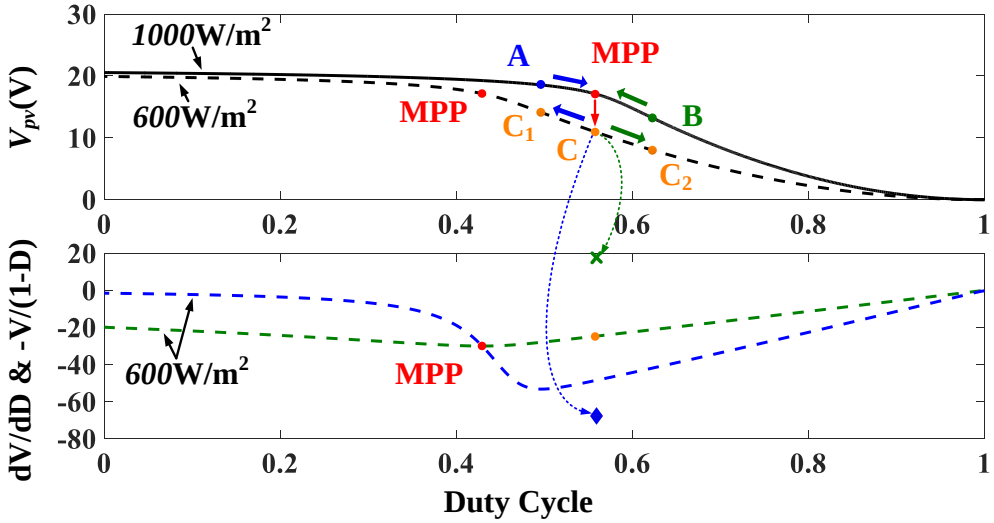


(a)

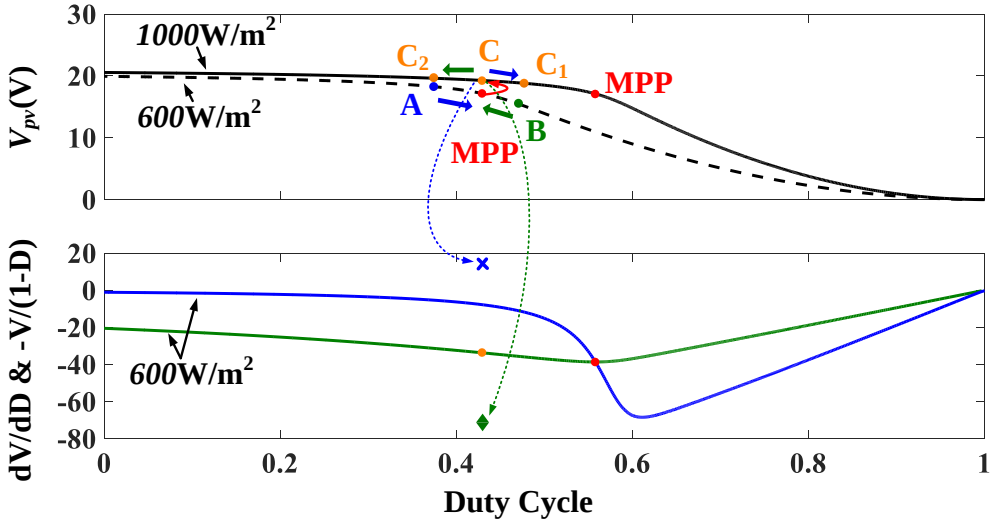


(b)

Fig. 3. Drift analysis for the SIVS method in [34]: (a) when solar irradiance decreases; (b) when solar irradiance increases.

decide the next perturbation direction, $sign$. In addition, the present values $V(\mathrm{k})$ and $D(\mathrm{k})$ are stored as the previous ones and the presented method starts again from the beginning.

In order to avoid the drift condition when the solar irradiance changes, additional operation conditions are used, which are marked in a red dash block in Fig. 5. According to TABLE II, it can be found that the drift phenomenon will happen when $\mathrm{d}D$ is negative, while the drift phenomenon will not happen when $\mathrm{d}D$ is positive. Therefore, the presented method will firstly detect whether $\mathrm{d}D$ is negative or not. If $\mathrm{d}D$ is not negative, $sign$ will not be changed. Otherwise, a further judgement will be made to detect

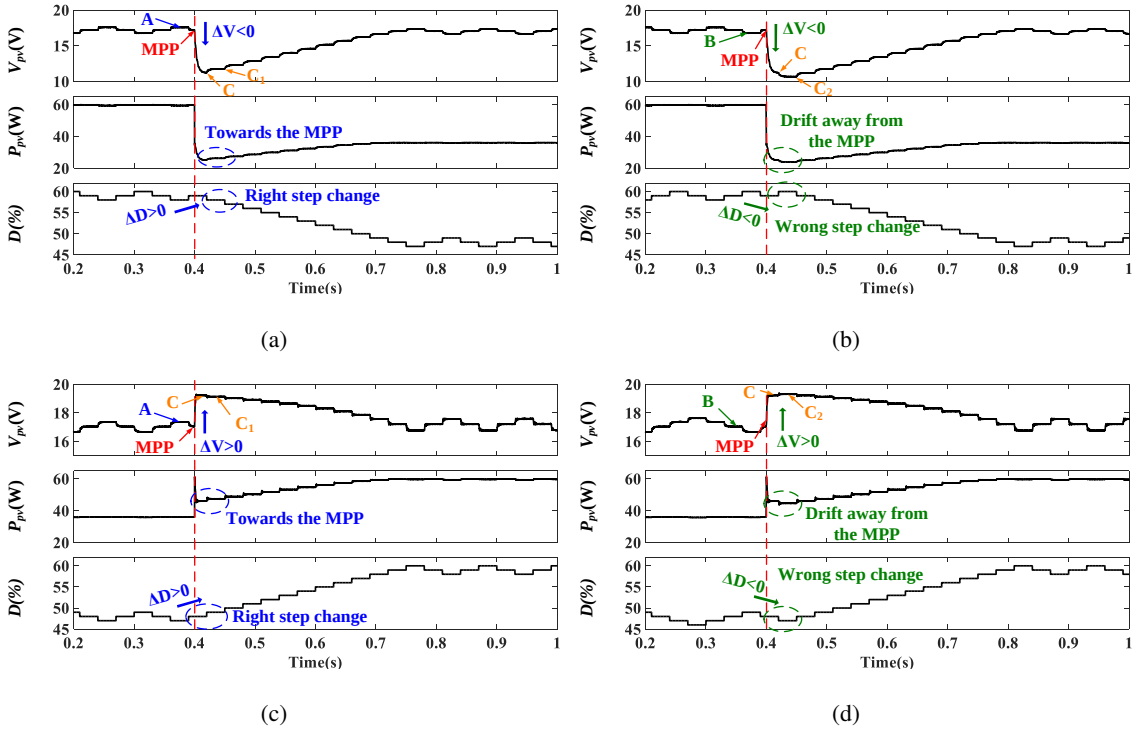


Fig. 4. Simulation results for the SIVS method in [34] when the solar irradiance changes between 1000W/m$^2$ to 600W/m$^2$. (a) No drift when the solar irradiance decreases; (b) Drift when the solar irradiance decreases; (c) No drift when the solar irradiance increases; (d) Drift when the solar irradiance increases.

TABLE II

VARIATION IN $\mathrm{d}V$, $\mathrm{d}D$ AND $D$ DURING THE VARIATION IN SOLAR IRRADIANCE

| Solar irradiance | $\mathrm{d}V$ | $\mathrm{d}D$ | $D$ | Drift |
|---|---|---|---|---|
| Decrease | negative | positive | Decrease | No |
| | | negative | Increase | Yes |
| Increase | positive | positive | Increase | No |
| | | negative | Decrease | Yes |

whether the solar irradiance changes.

As shown in Fig. 3 (a) and Fig. 4 (b), when solar irradiance decreases, $\mathrm{d}V$ is always negative. When both of $\mathrm{d}D$ and $\mathrm{d}V$ are negative, the drift will happen. Therefore, when both of the conditions $\mathrm{d}D < 0$ and $\mathrm{d}V < 0$ are satisfied, $sign$ will be changed to avoid the drift.

When the solar irradiance increases, the conditions for judgement is different and needs to specify

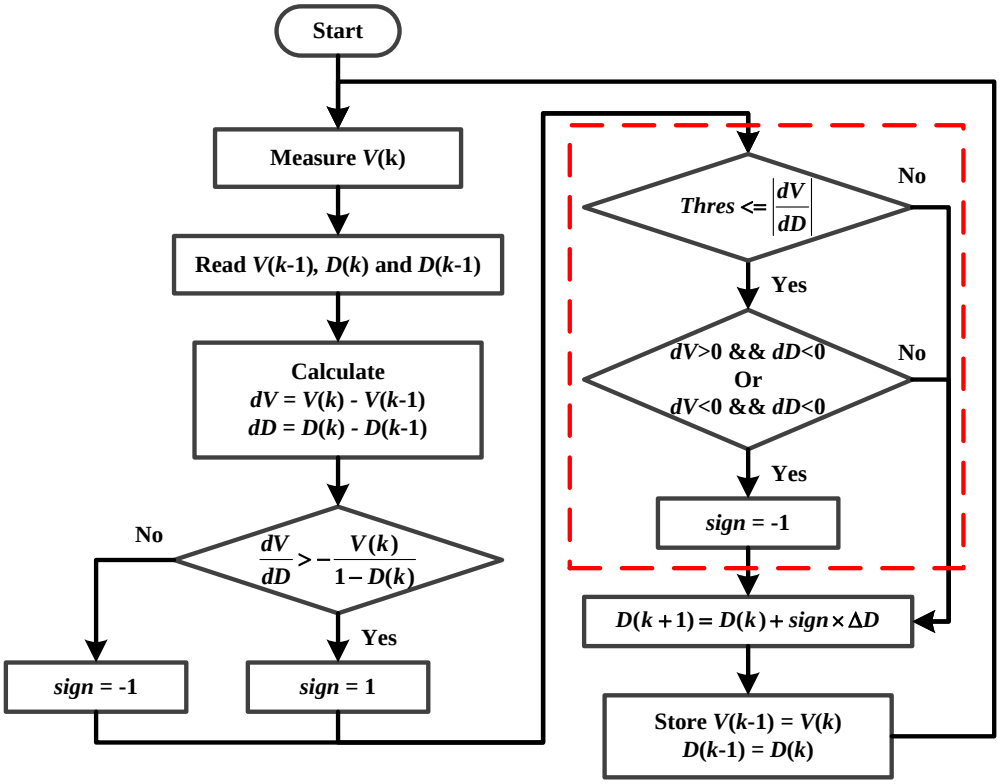


Fig. 5. Flowchart of the new method.

accordingly. As observed in Fig. 3 (b), the absolute value of the incremental parameter $|\mathrm{d}V/\mathrm{d}D|$ is significantly large when the solar irradiance increases. Thus, a threshold, $Thres$, is defined here to check whether the solar irradiance increases

$$Thres < \left(\left|\frac{\mathrm{d}V}{\mathrm{d}D}\right|_{G\uparrow}\right)_{min} \tag{16}$$

where $(|\frac{\mathrm{d}V}{\mathrm{d}D}|_{G\uparrow})_{min}$ refers to the minimal value of this incremental parameter caused by the increase of the solar irradiance.

### *C. Determination of the Threshold*

Generally, the step size $\mathrm{d}D$ in (16) can be either fixed [34] or variable [11, 15]. However, its value is not directly related to the increase of the solar irradiance. Therefore, the value of $(|\frac{\mathrm{d}V}{\mathrm{d}D}|_{G\uparrow})_{min}$ is mainly determined by $\mathrm{d}V$. In other words, the determination of $(|\frac{\mathrm{d}V}{\mathrm{d}D}|_{G\uparrow})_{min}$ is equivalent to the determination of $(\mathrm{d}V_{G\uparrow})_{min}$.

In order to analytically determine the value of $(\mathrm{d}V_{G\uparrow})_{min}$, the single-diode PV model is used, which can be written as below [3, 35]:

$$I = I_{ph} - I_0 \left[\exp\left(\frac{V + IR_s}{V_t} - 1\right)\right] - \frac{V + IR_s}{R_{sh}} \tag{17}$$

where $I$ and $V$ are the PV module current and voltage; $I_{ph}$ is the photovoltaic current; $I_0$ is the reverse saturation current of the diode; $R_s$ is the equivalent series resistance of the solar cell; $R_{sh}$ is the equivalent shunt resistance;$V_t$ is the junction thermal voltage, which can be written as $V_t = \frac{N_s kAT}{q}$, where $N_s$ is the number of the cells in the PV module; $q$ is the electron charge $1.602 \times 10^{-19}C$; $A$ is the diode ideality factor; $K$ is Boltzmann constant $1.38 \times 10^{-23}J/K$j T(in Kelvin) is the temperature of the $p$–$n$ junction.

For the operating point on the $I$-$V$ curve, it has:

$$R_{pv} = V/I, \quad I = V/R_{pv} \tag{18}$$

Substituting (18) into (17), (17) can be rewritten as

$$\frac{V}{R_{pv}} = I_{ph} + I_0 - I_0 \exp\left(\frac{V + (\frac{V}{R_{pv}})R_s}{V_t}\right) - \frac{V + (\frac{V}{R_{pv}})R_s}{R_{sh}} \tag{19}$$

Then, moving the term $[V + (\frac{V}{R_{pv}})R_s]/R_{sh}$ to the left side and multiplying both sides by $R_{sh}$ and $R_{pv}$, (19) can be rewritten as

$$\begin{aligned} V(R_{pv} + R_{sh} + R_s) = {} & R_{pv}R_{sh}(I_{ph} + I_0) \\ & - R_{pv}R_{sh}I_0 e^{\frac{V + (\frac{V}{R_{pv}})R_s}{V_t}} \end{aligned} \tag{20}$$

Taking $C_1 = (1 + R_s/R_{pv})/V_t$, (20) can be rewritten as

$$V = \frac{R_{pv}R_{sh}(I_{ph} + I_0) - R_{pv}R_{sh}I_0 e^{C_1 V}}{R_{pv} + R_{sh} + R_s} \tag{21}$$

By multiplying both sides by $C_1$, (21) can be rewritten as

$$C_1 V + \frac{C_1 R_{pv}R_{sh}I_0}{R_{pv} + R_{sh} + R_s} e^{C_1 V} = \frac{R_{pv}R_{sh}(I_{ph} + I_0)}{R_{pv} + R_{sh} + R_s} \tag{22}$$

Taking $C_2$ and $C_3$ as

$$C_2 = \frac{C_1 R_{pv}R_{sh}I_0}{R_{pv} + R_{sh} + R_s}, \quad C_3 = \frac{R_{pv}R_{sh}(I_{ph} + I_0)}{R_{pv} + R_{sh} + R_s} \tag{23}$$

(22) can be rewritten as

$$C_1 V + C_2 e^{C_1 V} = C_3 \tag{24}$$

Taking the exponential of both sides

$$e^{C_1 V} \cdot \exp\left(C_2 e^{C_1 V}\right) = e^{C_3} \tag{25}$$

TABLE III

MAIN PRODUCT PARAMETERS OF THE MSX-60W

| Parameter | Symbol | Value |
|---|---|---|
| Maximum power | $P_{mpp}$ | $60W$ |
| Voltage at maximum power | $V_{mpp}$ | $17.1V$ |
| Current at maximum power | $I_{mpp}$ | $3.5V$ |
| Open-circuit voltage | $V_{oc}$ | $21.1V$ |
| Short-circuit current | $I_{sc}$ | $3.8V$ |
| Temperature coefficient of $V_{oc}$ | $K_v$ | $-80mV/^{\circ}C$ |
| Temperature coefficient of $I_{sc}$ | $K_i$ | $0.065\%/^{\circ}C$ |

By multiplying both sides by $C_2$

$$C_2 e^{C_1 V} \cdot \exp\left(C_2 e^{C_1 V}\right) = C_2 e^{C_3} \tag{26}$$

Now, the first member is in the form $we^w$, then taking the Lambert W of both sides:

$$\begin{aligned} C_2 e^{C_1 V} &= W(C_2 e^{C_3}) \\ e^{C_1 V} &= W(C_2 e^{C_3})/C_2 \end{aligned} \tag{27}$$

Taking the logarithmic operation of both sides

$$\ln(e^{C_1 V}) = \ln(W(C_2 e^{C_3})/C_2) \tag{28}$$

Finally, (28) can be simplified as

$$V = \frac{\ln[W(C_2 e^{C_3})] - \ln(C_2)}{C_1} \tag{29}$$

In (29), some parameters, such as $R_s$, $R_{sh}$, $I_0$ and $A$, can be treated as constant values, while $I_{ph}$ and $R_{pv}$ are variable. In this paper, the PV module MSX-60W is used, where its main parameters are shown in TABLE III. Consequently, the values of $R_s$, $R_{sh}$, $I_0$ and $A$ are calculated as $0.387\Omega$, $161.075\Omega$, $2.452 \times 10^{-10}C$ and $0.974$, respectively, which are based on the National Renewable Energy Laboratory (NREL) System Advisor Model [4]. Therefore, $V$ is only related to $I_{ph}$ and $R_{pv}$, and not related to the converter topology or the load type. Then,(29) can be expressed as:

$$V = f(R_{pv}, I_{ph}) \tag{30}$$

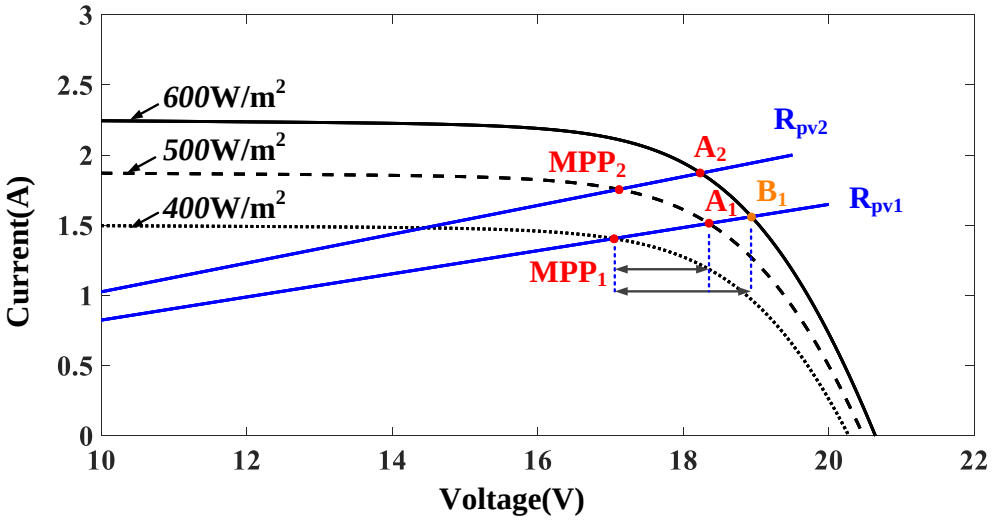


Fig. 6. The movement of the operating point on the $I$-$V$ curve when the solar irradiance increases.

Fig. 6 shows the movement of the operating point on the $I$-$V$ curve when the solar irradiance increases. When the solar irradiance increases within a given range, the load line, $R_{pv}$, has different values. For $I_{ph}$, it an be expressed as [35]:

$$I_{ph} \simeq I_{sc} = \frac{G}{G_{STC}}(K_I \Delta T + I_{sc,STC}) \tag{31}$$

where $G$ refers to the value of the solar irradiance, $\Delta T$ refers to the values of the temperature changes, $G_{STC}$ and $I_{sc,STC}$ refer to the values of $G$ and $I_{sc}$ at the standard test condition (STC), respectively. Since the temperature usually dose not change significantly in a short period, $\Delta T$ can be treated as zero. Hence, $I_{ph}$ is also related to the changes in the solar irradiance. As aforementioned discussion, $\mathrm{d}V_{G\uparrow}$ based on (30) can be expressed as:

$$\mathrm{d}V_{G\uparrow} = f(R_{pv}, G_2) - f(R_{pv}, G_1) \tag{32}$$

where $G_1$ and $G_2$ refer to the values before and after the solar irradiance changes, respectively. Here, the difference between $G_1$ and $G_2$ is defined as $\Delta G$.

In order to obtain $(\mathrm{d}V_{G\uparrow})_{min}$, $\Delta G$ needs to select properly. If $\Delta G$ is too large, the changes of the solar irradiance will be fast and the value of $\mathrm{d}V_{G\uparrow}$ will be large too. Since the minimum value of $\mathrm{d}V_{G\uparrow}$ needs to be obtained, $\Delta G$ cannot be too large. By contrast, if $\Delta G$ is too small, the solar irradiance will slightly change. It will be not necessary to set the threshold since the drift is not likely to happen under a slow change in the solar irradiance.

In order to determine $\mathrm{d}V_{G\uparrow}$, dynamic EN 50530 test standard is used to choose these values. As shown in Fig.7, the dynamic EN 50530 test procedure includes two sequences of different irradiance levels

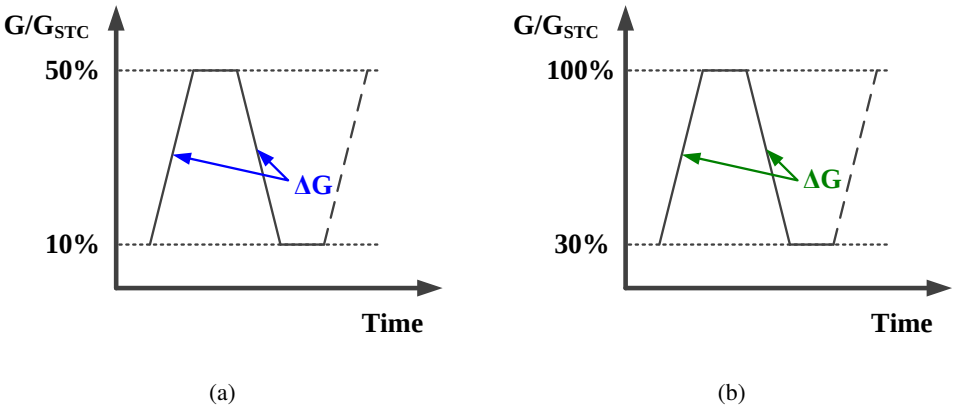


(a) (b)

Fig. 7. Dynamic EN 50530 test sequences procedure. (a) Sequence A; (b) Sequence B.

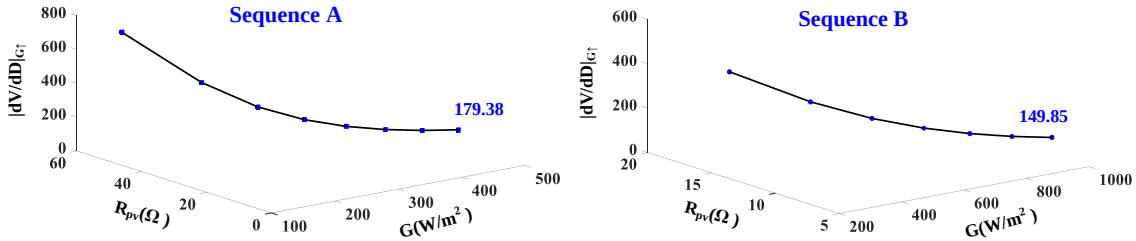


(a) (b)

Fig. 8. The different values of $|\frac{\mathrm{d}V}{\mathrm{d}D}|_{G\uparrow}$ under the dynamic EN 50530 test standard. (a) Sequence A; (b) Sequence B.

[2]. The sequence A fluctuates between $100W/m^2$ and $500W/m^2$, and sequence B fluctuates between $300W/m^2$ and $1000W/m^2$.

In this paper, $\Delta G$ for the sequence A and The sequence B are chosen as $50W/m^2$ and $100W/m^2$, respectively. Assuming $\mathrm{d}D$ is $0.5\%$, the different values of $|\frac{\mathrm{d}V}{\mathrm{d}D}|_{G\uparrow}$ under the dynamic EN 50530 test standard are given in Fig. 8.

From Fig. 8, it can be seen that the values of $|\frac{\mathrm{d}V}{\mathrm{d}D}|_{G\uparrow}$ under the lower solar irradiance are much larger than those under the higher solar irradiance. As shown in Fig. 8, the minimum values of $|\frac{\mathrm{d}V}{\mathrm{d}D}|_{G\uparrow}$ for the sequence A and the sequence B are 178.38 and 149.85, respectively. Therefore, in this paper, the threshold, $Thres$, is set as 120.

## IV. Experimental Results

An experimental prototype of the PV system was built up in order to verify the effectiveness of the presented method. Fig.9 shows the test bench of this PV system, which incudes boost converter, PV emulator, electronic load and a dSPACE controller. The PV emulator Chroma ATE-62050H-600S

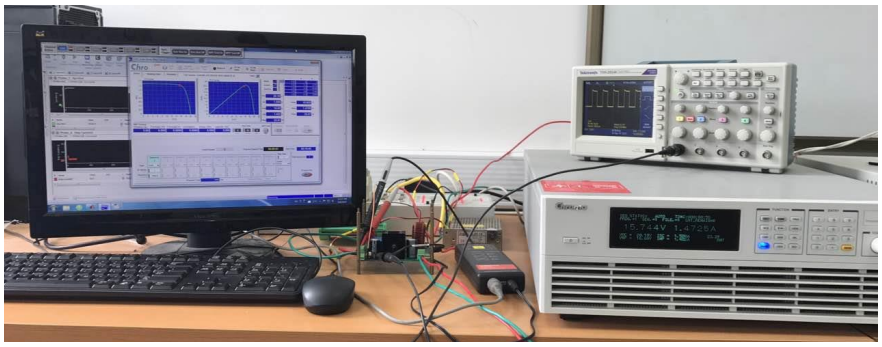

Fig. 9. Experimental prototype of the PV system with MPPT control.

was used to emulate solar array characteristics. The dSPACE DS1104 was used to implement the control algorithms of various MPPT methods. The electronic load IT8514C+ was used as the load. The parameters of boost converter is shown in TABLE IV. Besides, LV25-P is used for voltage sensor.

TABLE IV
MAIN COMPONENTS FOR THE BOOST CONVERTER

| Parameter | Value |
|---|---|
| Electrolytic capacitor (PV side) | 470uF |
| Electrolytic capacitor (Load side) | 47uF |
| Inductor L | 1mH |
| IGBT | IRG4PH50U |
| Diode | RHRG30120 |
| Voltage transducer | LV25-P |
| Switching frequency | 10kHz |

In order to validate the presented method, three different cases were designed. Case I is defined by the solar irradiance varying between $1000W/m^2$ and $800W/m^2$, which represents high-intensity irradiance. Case II is defined by the irradiance changing between $600W/m^2$ and $500W/m^2$, which represents moderate-intensity irradiance. For the Case III, the change range of irradiance is between $400W/m^2$ and $300W/m^2$, which represents low-intensity irradiance. The variations for the each case are repeated 10 times in every 10 seconds. The presented algorithm with variable step size is implemented and compared with the conventional SIVS method. The experimental results of the three cases are shown in Fig. 10, Fig. 11 and Fig. 12, respectively. It should be noted that the waveforms of power $P_{pv}$ are measured by the output of the PV emulator, and the waveforms of voltage $V_{pv}$ and duty cycle $D$ are

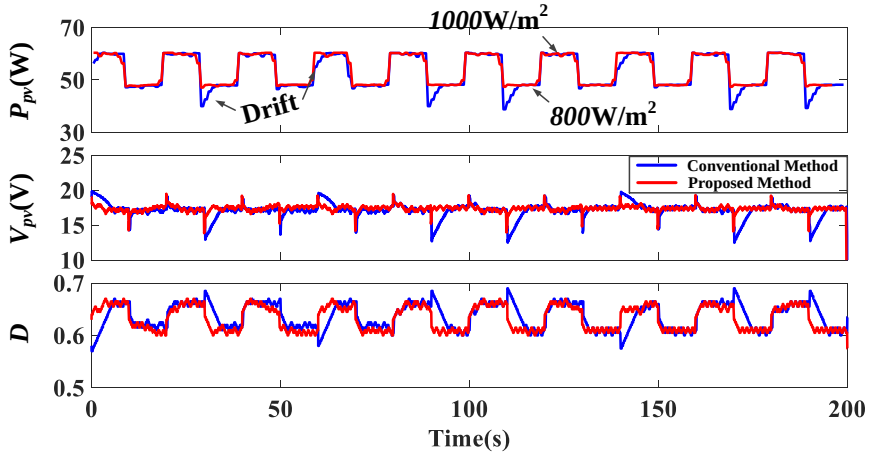


Fig. 10. Experimental results for case I.

recorded by the dSPACE.

As shown in Fig. 10, it is clearly seen that the conventional SIVS method, marked as blue colors, has 8 times drift in 20 times solar irradiance variations. Compared to the conventional SIVS method, the presented method, marked as red colors, has no drift for the same conditions. As a consequence, the tracking efficiencies for the conventional SIVS method and the presented method under the case I are 96.21% and 97.65%, respectively.

Similarly, there are 8 times and 9 times drift for the conventional SIVS method under the case II and the case III, respectively. The tracking efficiencies for the conventional SIVS method are 96.58% and 95.26% under the case II and the case III, respectively. The presented method does not have any drift happened under the same conditions. Therefore, the tracking efficiencies for the presented method are higher than those for the conventional SIVS method, which are 97.06% and 96.78% under the case II and the case III, respectively.

In order to explore the difference between these two methods, the zoomed views of the experimental results of the case II are shown in Fig. 13 and Fig. 14, which represent the increase and the decrease in the solar irradiance, respectively.

As shown in Fig. 13(a), the solar irradiance increases from $500W/m^2$ to $600W/m^2$ at the time instant of $80s$. At this instant, $\Delta D$ and $\Delta V$ are detected as negative and positive, respectively. Then, it is calculated that the term $\mathrm{d}V_{pv}/\mathrm{d}D$ is smaller than the term $-V_{pv}/(1-D)$. According to (6), $D$ should be decreased. As a consequence, a wrong step change is made by the conventional SIVS method, which causes the operating point drifts away from the MPP. Thus, the conventional SIVS method is required to use 15 steps to relocate the MPP. By contrast, the presented method detects that $Thres$ is smaller than

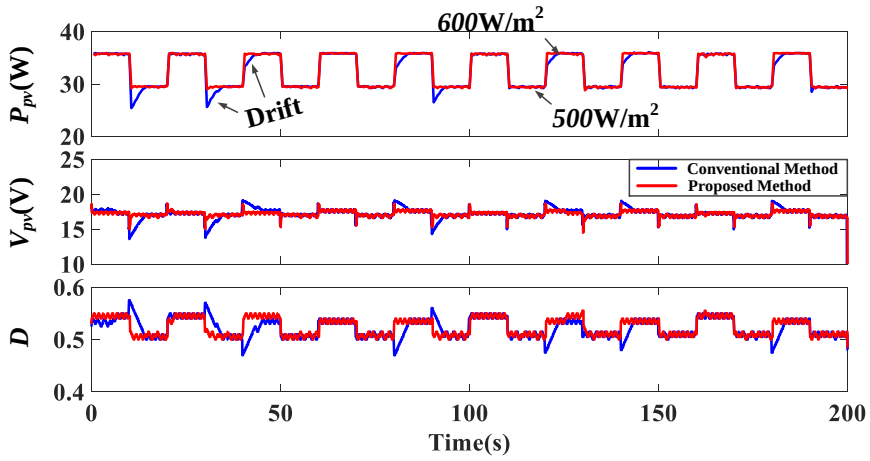


Fig. 11. Experimental results for case II.

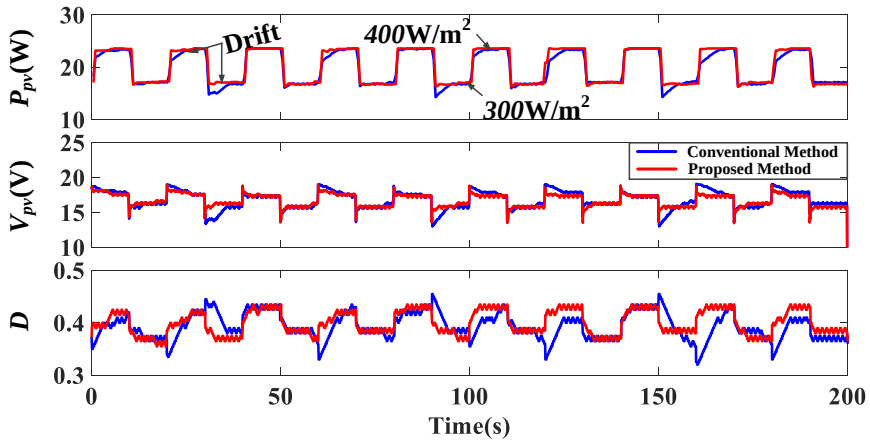


Fig. 12. Experimental results for case III.

the value of $\mathrm{d}V_{pv}/\mathrm{d}D$ at the time instant of $100s$. $sign$ is changed and a right step change is made to avoid the drift, as shown in Fig. 13(b). Therefore, only 2 steps are required to find the MPP.

In Fig. 14(a), both of $\Delta D$ and $\Delta V$ are detected as negative at the time instant of $30s$, when the solar irradiance decreases from $600W/m^2$ to $500W/m^2$. Then, it is calculated that the value of $\mathrm{d}V_{pv}/\mathrm{d}D$ is larger than that of $-V_{pv}/(1-D)$. Hence, a wrong step change is made again by the conventional SIVS method due to (6). As a result, the operating point drifts away from the MPP and 9 steps are required to locate the MPP. However, compared to the conventional SIVS method, the presented method detects both of the negative $\Delta D$ and $\Delta V$ and change $sign$. Therefore, the right step change is made to avoid the drift, and only 2 steps are needed, as shown in Fig. 14(b).

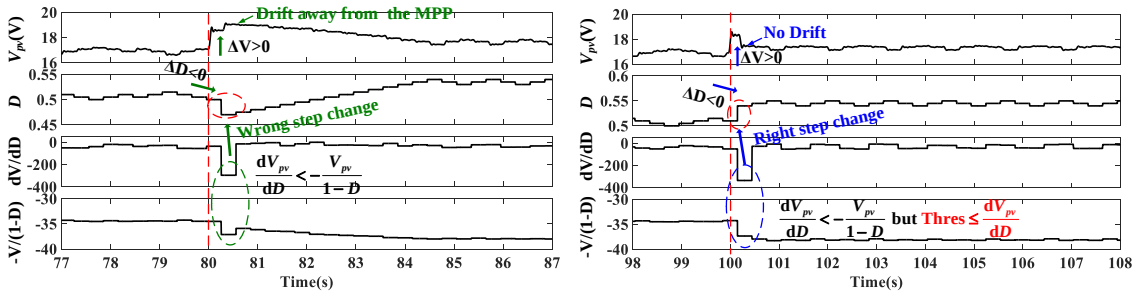


(a) (b)

Fig. 13. Zoomed view of the experimental results under the solar irradiance increasing (a) The conventional SIVS method; (b) The presented method.

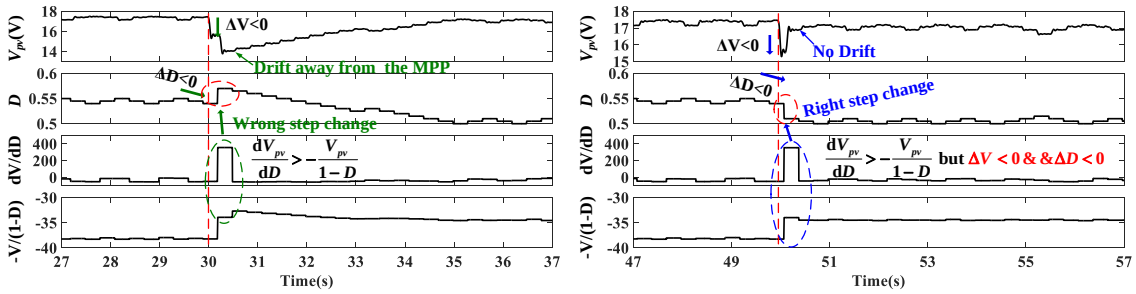


(a) (b)

Fig. 14. Zoomed view of the experimental results under the solar irradiance decreasing (a) The conventional SIVS method; (b) The presented method .

Finally, the summarization of experimental results are shown in TABLE V. It is clearly seen that there is no drift happened for the three cases by using the presented method. As a consequence, the tracking efficiencies of the presented method are generally higher than the conventional SIVS method. Furthermore, it should be note that the drift is randomly happened for the conventional SIVS method. Therefore, the drift probability for the conventional SIVS method is approximately equal to 50%.

## V. Conclusion

This paper presents a novel current sensorless (CS) maximum power point tracking (MPPT) algorithm that uses only one signle-input-voltage sensor (SIVS), which can significantly reduce the system cost. Furthermore, the drift phenomenon by using the conventional SIVS method is studied. The drift-free technique is adopted in the presented algorithm by incorporating the information of change in duty cycle ($\Delta$D) and change in input voltage ($\Delta$V). The corresponding criterion in realizing the drift-free operation is accurately expressed by the mathematical expression and the threshold is specified by the Lambert

TABLE V

SUMMARIZATION OF EXPERIMENTAL RESULTS

| Case | Methods | Drift Times | Total Times | Drift probability | Efficiency |
|---|---|---|---|---|---|
| I | SIVS | 8 | 20 | 40% | 96.21% |
| | Presented | 0 | 20 | 0% | 97.65% |
| II | SIVS | 8 | 20 | 40% | 96.58% |
| | Presented | 0 | 20 | 0% | 97.06% |
| III | SIVS | 9 | 20 | 45% | 95.26% |
| | Presented | 0 | 20 | 0% | 96.78% |

W function with respect to the dynamic EN50530 test standard. A comprehensive comparison between the presented algorithm and the conventional SIVS algorithm was carried out for different scenarios. Through the experimental results, it proves that the drift probability for the conventional SIVS method is approximately equal to 50%. Furthermore, it also validates the effectiveness of the presented algorithm, and its tracking efficiencies for the three cases are 97.65%, 97.06% and 96.78%, respectively, which are higher than those of the conventional method due to the avoidance of the drift phenomena.

## VI. ACKNOWLEDGEMENT

This work was supported by the Research development fund of XJTLU (RDF-16-01-10, RDF-17-01-28), the Jiangsu Science and Technology Programme (BK20161252), and the Suzhou Prospective Application programme (SYG201723), and the XJTLU Key Programme Special Fund (KSF-A-08).

## VII. REFERENCE

## REFERENCES

[1] Abdel-Salam, M., El-Mohandes, M.-T., Goda, M., 2018. An improved perturb-and-observe based mppt method for pv systems under varying irradiation levels. Sol. Energy 171, 547 – 561.

[2] Andrejasic, T., Jankovec, M., Topic, M., Jul. 2011. Comparison of direct maximum power point tracking algorithms using en 50530 dynamic test procedure. IET Renew. Power Gen. 5 (4), 281–286.

[3] Batzelis, E. I., Routsolias, I. A., Papathanassiou, S. A., Jan. 2014. An explicit pv string model based on the lambert w function and simplified mpp expressions for operation under partial shading. IEEE Trans. Sustain. Energy 5 (1), 301–312.

[4] Blair, N., Dobos, A., Freeman, J., Neises, T., Wagner, M., Ferguson, T., Gilman, P., Janzou, S., 2014. System advisor model, sam 2014.1. 14: General description. NREL Rep. No. TP-6A20-61019, Natl. Renew. Energy Lab. Golden, CO 13.

[5] Dallago, E., Finarelli, D. G., Gianazza, U. P., Barnabei, A. L., Liberale, A., Nov. 2013. Theoretical and experimental analysis of an mpp detection algorithm employing a single-voltage sensor only and a noisy signal. IEEE Trans. Power Electron. 28 (11), 5088–5097.

[6] Danandeh, M., G., S. M., 2018. Comparative and comprehensive review of maximum power point tracking methods for pv cells. Renew. Sust. Energy Rev. 82, 2743 – 2767.

[7] Dasgupta, N., Pandey, A., Mukerjee, A. K., Dec. 2008. Voltage-sensing-based photovoltaic mppt with improved tracking and drift avoidance capabilities. Sol. Energ. Mat. Sol. C. 92 (12), 1552–1558.

[8] Devi, V. K., Premkumar, K., Beevi, A. B., Ramaiyer, S., 2017. A modified perturb & observe mppt technique to tackle steady state and rapidly varying atmospheric conditions. Sol. Energy 157, 419 – 426.

[9] Femia, N., Petrone, G., Spagnuolo, G., Vitelli, M., Jul. 2005. Optimization of perturb and observe maximum power point tracking method. IEEE Trans. Power Electron. 20 (4), 963–973.

[10] Gotzens, F., Heinrichs, H., Hake, J.-F., Allelein, H.-J., 2018. The influence of continued reductions in renewable energy cost on the european electricity system. Energy Strategy Rev. 21, 71 – 81.

[11] Hua, C. C., Fang, Y. H., Chen, W. T., Feb. 2016. Hybrid maximum power point tracking method with variable step size for photovoltaic systems. IET Renew. Power Gen. 10 (2), 127–132.

[12] Jiang, Y., Qahouq, J. A. A., Haskew, T. A., Jul. 2013. Adaptive step size with adaptive-perturbation-frequency digital mppt controller for a single-sensor photovoltaic solar system. IEEE Trans. Power Electron. 28 (7), 3195–3205.

[13] Karami, N., Moubayed, N., Outbib, R., 2017. General review and classification of different mppt techniques. Renew. Sust. Energy Rev. 68, 1 – 18.

[14] Kasa, N., Iida, T., Chen, L., Aug. 2005. Flyback inverter controlled by sensorless current mppt for photovoltaic power system. IEEE Trans. Ind. Electron. 52 (4), 1145–1152.

[15] Killi, M., Samanta, S., Dec. 2015. An adaptive voltage-sensor-based mppt for photovoltaic systems with sepic converter including steady-state and drift analysis. IEEE Trans. Ind. Electron. 62 (12), 7609–7619.

[16] Killi, M., Samanta, S., Sep. 2015. Modified perturb and observe mppt algorithm for drift avoidance in photovoltaic systems. IEEE Trans. Ind. Electron. 62 (9), 5549–5559.

[17] Li, X., Wen, H., Hu, Y., Jiang, L., 2019. A novel beta parameter based fuzzy-logic controller for photovoltaic mppt application. Renew. Energy 130, 416 – 427.

[18] Li, X., Wen, H., Jiang, L., Hu, Y., Zhao, C., Sep. 2016. An improved beta method with auto-scaling factor for photovoltaic system. IEEE Trans. Ind. Appl. 52 (5), 4281–4291.

[19] Li, X., Wen, H., Jiang, L., Xiao, W., Du, Y., Zhao, C., Nov. 2016. An improved mppt method for pv system with fast-converging speed and zero oscillation. IEEE Trans. Ind. Appl. 52 (6), 5051–5064.

[20] Metry, M., Shadmand, M. B., Balog, R. S., Abu-Rub, H., Mar. 2017. Mppt of photovoltaic systems using sensorless current-based model predictive control. IEEE Trans. Ind. Appl. 53 (2), 1157–1167.

[21] Pandey, A., Dasgupta, N., Mukerjee, A. K., Mar. 2007. A simple single-sensor mppt solution. IEEE Trans. Power Electron. 22 (2), 698–700.

[22] Rajesh, R., Mabel, M. C., 2014. Efficiency analysis of a multi-fuzzy logic controller for the determination of operating points in a pv system. Sol. Energy 99, 77 – 87.

[23] Ram, J. P., Babu, T. S., Rajasekar, N., 2017. A comprehensive review on solar pv maximum power point tracking techniques. Renew. Sust. Energy Rev. 67, 826 – 847.

[24] S., S. E., Chatterjee, K., Bandyopadhyay, S., Mar. 2013. One-cycle-controlled single-stage single-phase voltage-sensorless grid-connected pv system. IEEE Trans. Ind. Electron. 60 (3), 1216–1224.

[25] Salas, V., Olias, E., Lazaro, A., Barrado, A., May. 2005. New algorithm using only one variable measurement applied to a maximum power point tracker. Sol. Energ. Mat. Sol. C. 87 (1), 675–684.

[26] Seo, G. S., Shin, J. W., Cho, B. H., Lee, K. C., Feb. 2014. Digitally controlled current sensorless photovoltaic micro-converter for dc distribution. IEEE Trans. Ind. Informat. 10 (1), 117–126.

[27] Sera, D., Teodorescu, R., Hantschel, J., Knoll, M., Jul. 2008. Optimized maximum power point tracker for fast-changing environmental conditions. IEEE Trans. Ind. Electron. 55 (7), 2629–2637.

[28] Shahid, H., Kamran, M., Mehmood, Z., Saleem, M. Y., Mudassar, M., Haider, K., 2018. Implementation of the novel temperature controller and incremental conductance mppt algorithm for indoor photovoltaic system. Sol. Energy 163, 235 – 242.

[29] Sher, H. A., Murtaza, A. F., Noman, A., Addoweesh, K. E., Al-Haddad, K., Chiaberge, M., Oct. 2015. A new sensorless hybrid mppt algorithm based on fractional short-circuit current measurement and p&o mppt. IEEE Transactions on Sustainable Energy 6 (4), 1426–1434.

[30] Sivakumar, P., Kader, A. A., Kaliavaradhan, Y., Arutchelvi, M., 2015. Analysis and enhancement of pv efficiency with incremental conductance mppt technique under non-linear loading conditions. Renew. Energy 81, 543 – 550.

[31] Sokolov, M., Shmilovitz, D., Dec. 2008. A modified mppt scheme for accelerated convergence. IEEE Trans. Energy Convers. 23 (4), 1105–1107.

[32] Soon, T. K., Mekhilef, S., 2014. Modified incremental conductance mppt algorithm to mitigate inaccurate responses under fast-changing solar irradiation level. Sol. Energy 101 (0), 333–342.

[33] Soon, T. K., Mekhilef, S., Feb. 2015. A fast-converging mppt technique for photovoltaic system under fast-varying solar irradiation and load resistance. IEEE Trans. Ind. Informat. 11 (1), 176–186.

[34] Urayai, C., Amaratunga, G. A. J., Feb. 2013. Single-sensor maximum power point tracking algorithms. IET Renew. Power Gen. 7 (1), 82–88.

[35] Villalva, M., Gazoli, J., Filho, E., May. 2009. Comprehensive approach to modeling and simulation of photovoltaic arrays. IEEE Trans. Power Electron. 24 (5), 1198–1208.